Dynamical color correlations in a $SU(2)_c$ quark exchange model of nuclear matter

S. Gardner* and C. J. Horowitz†
Nuclear Theory Center and Department of Physics, Indiana University, Bloomington, Indiana 47405

J. Piekarewicz‡
Supercomputer Computations Research Institute, Florida State University, Tallahassee, Florida 32306
(Received 27 December 1993)

The quark exchange model is a simple realization of an adiabatic approximation to the strong-coupling limit of quantum chromodynamics: the quarks always coalesce into the lowest energy set of flux tubes. Nuclear matter is thus modeled in terms of its quarks. We wish to study the correlations imposed by total wave-function antisymmetry when color degrees of freedom are included. To begin with, we have considered one-dimensional matter with a SU(2) color internal degree of freedom only. We proceed by constructing a totally antisymmetric, color singlet *Ansatz* characterized by a variational parameter λ (which describes the length scale over which two quarks in the system are clustered into hadrons) and by performing a variational Monte Carlo calculation of the energy to optimize λ for a fixed density. We calculate the q-q correlation function as well, and discuss the qualitative differences between the system at low and high density.

PACS number(s): 24.85.+p, 21.65.+f, 12.39.Jh

I. INTRODUCTION

With the advent of new, high-energy facilities for nuclear physics research (CEBAF, RHIC), the issue of identifying departures from a conventional, meson-baryon description of nuclear phenomena presses. One would naively expect that as the typical distance scales probed become short—relative to the radius of the proton—that the fundamental ingredients of the strong interaction, namely, the quarks and gluons, should become manifest in nuclear observables. This has not been the case. Indeed, unambiguous signatures of the formation of a "quark-gluon plasma" (QGP), hoped for at RHIC, have proven elusive. The fickleness of many newly proclaimed signatures stems from the disparate pictures of observables in the quark/gluon or hadronic viewpoints. For example, J/ψ suppression was heralded as a clear signature of QGP formation [1], yet it seems that suppression can also be realized in a hadronic description of high density matter at high temperatures without plasma formation [2,3]. The divorce of the two pictures is perhaps forced by the difficulty of treating quark confinement. We offer no new insight into this technical problem; rather, we argue that it is useful to consider a simple model which interpolates between a hadron-based and quark-based description at low and high density.

In this paper, we shall consider nuclear matter from the viewpoint of a constituent quark model. The particular model we use, the quark exchange model, has "natural" low and high-density limits: it behaves as a system of isolated hadrons at low density and as a nonrelativistic Fermi gas of quarks at high density. Our purpose is to attempt to understand the structure of nuclear matter in terms of its quarks. Potentially, we would like to understand traditional issues, such as nuclear binding and saturation, from a quark model viewpoint. We anticipate that some "duality" may exist between the quark-gluon and hadronic descriptions. Indeed, the study of this quark-based description at nuclear matter density should help us to identify to what extent the descriptions are equivalent. However, this is not our sole purpose. In our, albeit simple, model, the structure of the system at fixed density is controlled entirely by the quark exchange dynamics, rather than by approximations to the hadronic and quark-based phases which are neither obviously consistent nor compatible. Consequently, we regard the study of the structure of the system with density as the major focus of our study. We hope to gain insight into the nature of a quark-hadron phase transition, as well as into the system's structure above and below the supposed transition point. In principle, our study also allows us to search for new collective excitations of the system, which could be novel in structure and unique to the quark-based description. However, we shall not explore such venues here.

The model we use is the quark exchange model [4]. The quark exchange model is a nonrelativistic, potential model, with many-body, confining forces. The many-body nature of the interactions allows the saturation of the hadron-hadron forces—there are no long-range hadron-hadron forces in nature—to be imposed by fiat. The original quark exchange model [4] was constructed for the $q^2\bar{q}^2$ system in three spatial dimensions and in

*Electronic mail address: gardner@iucf.indiana.edu
†Electronic mail address: charlie@iucf.indiana.edu
‡Electronic mail address: jorgep@scri.fsu.edu

U(1) color. In this model, the U(1) limit is still confining, and the system studied shows rich behavior. For example, the symmetric spatial state possesses a weakly bound state. The binding energy's weakness, compared to the hadron confinement scale, is reminiscent of the deuteron. As a result, this model has been used in several previous quark model studies of nuclear matter and of finite many-quark systems [5–12]. For the most part, the studies are confined to one-spatial dimension and retain the restriction to U(1) color as well. These studies are of "spin zero fermions": spin is not explicitly treated, so that the spatial wave functions are required to be manifestly antisymmetric. This has the unfortunate effect of generating nuclear matter based on hadrons in parity-odd states. Horowitz and Piekarewicz have extended their work in one dimension [6] to three dimensions and have, in addition, considered an approximate extension to SU(3) color [7]. The studies, for the most part, rely heavily on variational Monte Carlo methods; however, the authors of Ref. [9] use a two-body reduction of the many-body Hamiltonian of Ref. [4], so that they can use conventional many-body techniques.

This work is concerned with the complete treatment of color degrees of freedom, and with the resulting structure of the system's ground state. In our model, the gluon degrees of freedom are passive—they act only to confine the quarks, so that they cannot be excited. Only the quarks, then, carry an explicit color label; our treatment is "complete" in this context. As in previous papers, we shall continue to ignore the quarks' spin. As we do include color, though, nuclear matter is based on parity-even hadron states, as desired. A full treatment of color necessarily implies enumeration of all the exchange terms required for the construction of a fully antisymmetric state for a finite number of quarks. This necessity limits this initial study to SU(2) color and one spatial dimension for tractability. We believe, however, that the techniques presented here can be extended to SU(3) color and three spatial dimensions.

The simple model we use has many shortcomings: it is not relativistic, even at high density, and there is no mechanism for the production and propagation of virtual $q\bar{q}$ pairs. Moreover, chiral symmetry has no meaning. Yet, we believe that the model study presented here gives useful insight into the nature of hadronic matter as a function of density. The model does include the effects of confinement and antisymmetry, and its virtue is that the structure of the system as a function of density is determined by this physics. To some extent, our results can be understood in terms of the interplay of these two effects. The qualitative insight we gain as a result should be relevant in understanding the predictions of richer models, as the effects we have included, confinement and antisymmetry, surely play no minor role.

Section II summarizes the U(1) quark exchange model, and Sec. III describes its extension to SU(2) color. We compare our model with other models of color in Sec. IV, before proceeding, in Sec. V, to describe the Monte Carlo computations. Our results are summarized in Sec. VI, and we conclude with an outlook towards future work in Sec. VII.

II. THE QUARK EXCHANGE MODEL

Here we describe the quark exchange model. For two isolated quarks in one spatial dimension, we consider the Hamiltonian

$$H = -\frac{1}{2}\partial_1^2 - \frac{1}{2}\partial_2^2 + \frac{1}{2}(x_1 - x_2)^2 \ . \tag{2.1}$$

The units have been chosen such that the quark mass m_q and the oscillator frequency ω are $m_q = \hbar = \omega = 1$. We shall consider harmonic confinement exclusively, merely for tractability. The potential term can be thought of as a flux tube which confines quarks 1 and 2. For N quarks, we wish to generalize the potential term so that confining potentials "connect" the quarks to yield the lowest possible potential energy. We shall avoid any explicit discussion of color for the moment, and simply require that the quark "links" act in a pairwise fashion. Following Horowitz *et al.* [5], the Hamiltonian for N quarks becomes

$$H = -\frac{1}{2}\sum_{i=1}^{N}\partial_i^2 + V(x_1, \ldots, x_N) \ , \tag{2.2}$$

where the potential $V(x_1, \ldots, x_N)$ is

$$V(x_1, \ldots, x_N) = \min_{[P]} V_P(x_1, \ldots, x_N), \tag{2.3}$$

such that

$$V_P(x_1, \ldots, x_N) \equiv \sum_{i=1}^{N/2} v(x_{P^{2i-1}} - x_{P^{2i}}), \tag{2.4}$$

with $v(x_{P^1} - x_{P^2}) = (x_{P^1} - x_{P^2})^2/2$. The P are elements of the permutation group S_N, where P^i is the ith member of the element P. In this way, all possible pairwise confining potentials are sampled.

As the potential requires that the quarks be paired in a way that the global potential energy is minimized, the model is driven by quark exchange dynamics. That is, slight changes in the spatial configurations of the quarks may result in rearrangements of the links which confine them. The exchange of quarks between links is the only dynamical feature of the model. These dynamics are illustrated schematically in Fig. 1.

The advantage of the simple prescription of Eq. (2.3) is that cluster separability is guaranteed. By "cluster separability," we mean that no long-range, residual forces exist between color-singlet clusters at large separations. Such color van der Waals forces do not exist in nature [13], so that cluster separability is a desirable property. Yet in all models with pairwise, confining forces, color van der Waals forces (dipole-dipole interactions) do exist [14]. The potential of Eq. (2.3) succeeds in providing cluster separability because the forces are of an intrinsically many-body nature.

In some sense, Eq. (2.3) represents an adiabatic approximation to a strong coupling picture of quark-quark interactions. The gluon degrees of freedom, which are inert, act as links which connect the quarks to yield the low-

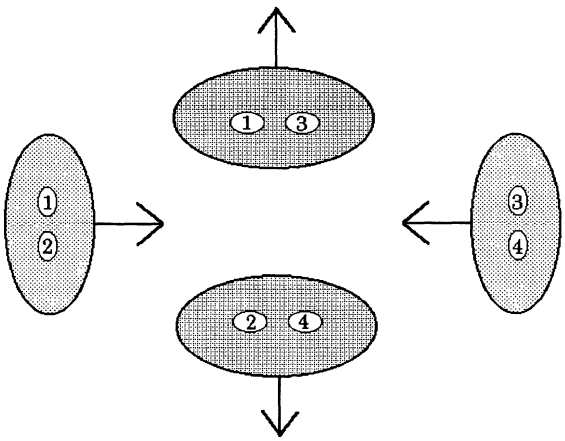

FIG. 1. An illustration of quark exchange dynamics for four quarks. Two incoming hadrons with quark content $(12)_0$ and $(34)_0$ may exchange quarks—the strings connecting 1 to 2 and 3 to 4 flip—to yield a $(13)_0(24)_0$ outgoing state.

est potential energy. We do not include the possibility of gluonic excitation in our model; the absence of low-lying $q\bar{q}$ states with exotic quantum numbers [15] supports this model choice. The interaction is adiabatic, as the links rearrange themselves instantaneously in adjustment to the configuration of the quarks. This picture relies on a separation of time-scale between the quark and gluon degrees of freedom in QCD. This is not unreasonable for heavy quarks; this is, fortunately, the same limit in which the nonrelativistic quark model, which is also used here, has validity. For realistic, two-flavor quark matter, these approximations are not obviously robust; we adopt them out of necessity.

The nonrelativistic quark model has been justified *a posteriori* by its phenomenological success in reproducing a broad range of baryon properties [16]. In addition, the U(1) $q^2\bar{q}^2$ model of Lenz *et al.* [4] evinces appealing qualitative behavior. As mentioned earlier, a weak bound state—compared to the confinement scale—exists in three dimensions. This scale is reminiscent of the deuteron. There also exist hidden channel resonances in the elastic phase shift, which occur at the hadronic inelastic channel thresholds. Yet, significant corrections to the adiabatic picture on which the Lenz *et al.* model is based likely exist. Existing studies focus on the N-N system, which suggest that the corrections are not small [17,18]. The simple Lenz *et al.* model does have interesting physics content, so that we shall proceed to explore it in an extension to quark matter in SU(2) color.

III. MAGIC MODEL IN SU(2) COLOR

Here, we shall consider SU(2) color quark matter in one spatial dimension, although we shall continue to ignore the quarks' spins. We want to extend the model above in such a way that the ground state is guaranteed to be an overall color singlet and that the system reduces at low density to color-singlet hadron clusters. These constraints are not sufficient to specify the extension to SU(2) color uniquely. Starting with the U(1) potential of Eq. (2.3), one possible extension is

$$V_{\mathrm{SU}(2)}(x_1,\ldots,x_N) = \left[\min_{[P]} V_P(x_1,\ldots,x_N)\right] \times \left(\alpha + 1 - \alpha P_{[P_{\min}]_0}\right) , \qquad (3.1)$$

where $P_{[P_{\min}]_0}$ denotes a color singlet state projector for the minimum energy pairing and α is a large and positive constant. For the pairing 12 34 56 78 . . .,

$$P_{[P_{\min}]_0} = |(12)_0\ (34)_0\ (56)_0\ (78)_0 \cdots\rangle\langle(12)_0\ (34)_0\ (56)_0\ (78)_0 \cdots| \, . \qquad (3.2)$$

The potential choice in Eq. (3.1) yields the required low-density limit of color-singlet hadron clusters. The constant α must be large relative to the maximum value of the spatial part of the potential, that is, large relative to $\left[\min_{[P]} V_P(x_1,\ldots,x_N)\right]$, in order for the prescription to be sensible. The simulations are performed for quarks in a box of length L under (anti)periodic boundary conditions, so that the spatial potential is bounded for fixed L. The state $|(12)_0\ (34)_0\ (56)_0\ (78)_0 \cdots\rangle$ is a manifest color singlet, though it is only a single component of the full antisymmetric wave function for the quarks. One must begin, then, with a Slater determinant for the initial wave function in order to guarantee antisymmetry under the exchange of any two quarks. This is no difference from the U(1) calculation. The SU(2) prescription given by Eqs. (3.1) and (3.2) effectively neglects any contribution to the wave function from paired triplet states which are coupled to an overall singlet. The so-called "hidden color" components of the wave function, then, are zero in this prescription.

Computing observables with the color projector of Eq. (3.2) is cumbersome at best, and there is no reason to demand that the quarks in each flux tube be in a local color singlet. We shall choose, then, a different SU(2) extension for use in this paper. We shall retain the original U(1) form of the potential, Eq. (2.3), to write

$$V_{\mathrm{magic}}(x_1,\ldots,x_N) = \left[\min_{[P]} V_P(x_1,\ldots,x_N)\right] \times (\alpha + 1 - \alpha P_0) \, . \qquad (3.3)$$

Note that P_0 now defines the projector on an *overall* color singlet. As before, α is a large and positive constant. In this case, however, the constant α does not really enter, as we can merely use a variational *Ansatz* which is an overall color singlet. Indeed, we shall require our variational *Ansatz* to satisfy the following contraints.

(i) The total wave function must be antisymmetric under quark exchange.

(ii) The total wave function must be a color singlet.

(iii) The total wave function must separate into color singlet hadron clusters as pairs of quarks are pulled apart.

The first two constraints are dictated by the structure of Eq. (3.3). The last constraint, however, is not—although it is certainly a necessary requirement for any reasonable model of confinement. Evidently, a single-channel model Hamiltonian does not suffice, yet adopting a Hamiltonian which depends on the coupling of the colors of the quarks is awkward. By adopting the above simple Hamiltonian with an *Ansatz* which obeys all the above constraints, we have declared that the flux-tube dynamics are such that these properties are simply *guaranteed.* For that reason, we call our extension to $SU(2)_c$ the "magic" model. This model choice implies that hidden color forces are now finite. The treatment of hidden color here is compared with previous treatments of color in the quark exchange model in Sec. IV.

Here we consider the case of SU(2) color and one spatial dimension for simplicity. We regard this specific case as a stepping stone to a more realistic calculation. Yet, it is the case that in one spatial dimension we can compare our constituent quark model to the nonrelativistic limit of QCD with one space and one time dimension, denoted as 1+1 QCD or QCD_2 [19]. QCD_2 is a confining theory, yet the mechanism of confinement is rather different from that supposed in three spatial dimensions (QCD_4). Indeed, confinement in QCD_2 is automatic, as the static Coulomb potential in one spatial dimension is linearly confining. It is for this reason that QCD_2 can be solved accurately in the weak coupling limit: the lowest-order terms include confinement, so that the ignored higher-order contributions generate quantitative, rather than qualitative, changes. This is distinct from QCD_4, in which confinement is a distinctly nonperturbative phenomenon. In QCD_2, in the weak coupling limit in axial gauge, assuming the meson to be a pure $q\bar{q}$ state, one can construct a Bethe-Salpeter equation for the meson state [20]. In the nonrelativistic limit, the Bethe-Salpeter amplitude satisfies a Schrödinger equation with a linear confining potential in the relative coordinate. Thus, our use of harmonic confinement is an approximation of convenience in QCD_2 as well.

Studies of QCD_2, however, need not be limited to the meson sector. One can study the extreme weak-coupling limit for N quarks as well [21] by considering the N quarks on a circle of length L in Coulomb gauge [22]. In this formulation, the infrared ambiguities of the axial gauge approach do not appear [23], so that both the color singlet and "hidden color" color singlet sectors can be studied. This is germane to our above difficulty, as the supposed asymptotic behavior of the "hidden color" portion of the Hamiltonian as paired triplet states are pulled apart generates the third constraint we impose on our variational *Ansatz.* The study of nonrelativistic QCD_2 for four quarks in $SU(2)_c$ yields a Schrödinger-type Hamiltonian with the following effective potential [21]. Here the quarks are ordered as $x_1 < x_2 < x_3 < x_4$, and the limit $L \to \infty$ has been taken:

$$V_0 = \frac{3}{8}g^2(x_4 - x_3) + \frac{3}{8}g^2(x_2 - x_1) \tag{3.4}$$

$$V_1 = g^2\left(\frac{x_4 + x_3}{2} - \frac{x_2 + x_1}{2}\right) - \frac{1}{8}g^2(x_4 - x_3) - \frac{1}{8}g^2(x_2 - x_1)\,. \tag{3.5}$$

Note that V_0 is the potential in the sector $|(12)_0(34)_0\rangle$, whereas V_1 is the potential in the "hidden color" sector $|(12)_1(34)_1\rangle_0$. The coupling constant in QCD_2 is g. One can repeat the above analysis for other quark orderings as well to conclude that the singlet-singlet sector potential is of quark-exchange-model form, that is, as given by Eqs. (2.3) and (2.4) with linear, rather than harmonic, strings [21]. Note, moreover, that the form of Eq. (3.5) guarantees that the state with (12) and (34) held at asymptotic separation is a singlet-singlet state, i.e., $|(12)_0(34)_0\rangle$. Thus, the constraint we impose on our variational *Ansatz* is consistent with QCD_2 as well.

We can also evaluate the consequences of our "magic model" prescription of using the singlet-singlet-sector Hamiltonian in concert with a variational *Ansatz* satisfying the above constraints to calculate the total energy of the global-color-singlet state. The issue is whether

$$\langle\Psi|V_0P_0 + V_1P_1|\Psi\rangle \tag{3.6}$$

is well approximated by

$$\langle\Psi_A|V_0|\Psi_A\rangle\,, \tag{3.7}$$

where

$$P_0 \equiv |(12)_0(34)_0\rangle\langle(12)_0(34)_0|,$$

$$P_1 \equiv |(12)_1(34)_1\rangle_{0\,0}\langle(12)_1(34)_1|,$$

and $|\Psi_A\rangle$ is the variational *Ansatz.* The normalization of the kets is such that $P_0^2 = P_0$ and $P_1^2 = P_1$. Now the exact wave function $|\Psi\rangle$ must be of the form

$$\begin{aligned}|\Psi\rangle &= f_{1234}|(12)_0(34)_0\rangle - f_{1324}|(13)_0(24)_0\rangle + f_{1423}|(14)_0(23)_0\rangle \\ &\equiv \left(f_{1234} - \frac{1}{2}f_{1324} - \frac{1}{2}f_{1423}\right)|(12)_0(34)_0\rangle - \frac{\sqrt{3}}{2}\left(f_{1324} - f_{1423}\right)|(12)_1(34)_1\rangle_0\,,\end{aligned} \tag{3.8}$$

where f_{ijkl} is symmetric under $x_i \leftrightarrow x_j$ or $x_k \leftrightarrow x_l$ exchange and is assumed to be real. The structure of Eq. (3.8) follows for any color singlet state comprised purely of fermions, so that $|\Psi_A\rangle$ has the same structure. In this case, f_{ijkl} is replaced by f^A_{ijkl}. Consequently,

$$\langle\Psi|V_0P_0+V_1P_1|\Psi\rangle=\langle f_{1234}|V_0|f_{1234}\rangle-\langle(f_{1324}+f_{1423})|V_0|f_{1234}\rangle+\langle f_{1324}|V_0|f_{1423}\rangle$$
$$+\langle(f_{1324}-f_{1423})|\tilde{V}_1|(f_{1324}-f_{1423})\rangle\,, \tag{3.9}$$

whereas

$$\langle\Psi_A|V_0|\Psi_A\rangle=\langle f^A_{1234}|V_0|f^A_{1234}\rangle-\langle(f^A_{1324}+f^A_{1423})|V_0|f^A_{1234}\rangle+\langle f^A_{1324}|V_0|f^A_{1423}\rangle$$
$$+\langle(f^A_{1324}-f^A_{1423})|V_0|(f^A_{1324}-f^A_{1423})\rangle\,. \tag{3.10}$$

Note that $\tilde{V}_1$ is $3g^2[(x_4+x_3)/2-(x_2+x_1)/2]/4$ for $x_1<x_2<x_3<x_4$. In making the magic-model prescription, then, we assume, for this ordering, say, that

$$\frac{3}{8}g^2(x_4+x_3-x_1-x_2)(f_{1324}-f_{1423})^2\approx\frac{3}{8}g^2(x_4+x_2-x_3-x_1)(f^A_{1324}-f^A_{1423})^2\,. \tag{3.11}$$

Certainly, in the limit where $(x_4-x_3)-(x_2-x_1)\gg(x_2-x_1)+(x_4-x_3)$, agreement is guaranteed, as both terms are small. Moreover, in the region where $(x_4-x_3)-(x_2-x_1)\gtrsim(x_2-x_1)+(x_4-x_3)$, so that the wave functions do not force the agreement to exist, the functions $(x_4+x_3-x_1-x_2)$ and $(x_4+x_2-x_3-x_1)$ are comparable. As long as $(f_{1324}-f_{1423})$ and $(f^A_{1324}-f^A_{1423})$ fall rapidly as $(x_4-x_3)-(x_2-x_1)$ grows large, the prescription we have used to estimate the total energy should be reasonable. Thus, we conclude that our model contains many features reminiscent of QCD_2 and is also remarkably more tractable, as no explicit projections on specific color states are required.

We shall now proceed to construct the desired variational *Ansatz*, and shall illustrate the procedure to come by considering the following *Ansatz* for four quarks:

$$\Psi^{4q}_{\rm trial}(x_1,x_2,x_3,x_4)=\exp[-\lambda(x_1-x_2)^2-\lambda(x_3-x_4)^2]\,f^{\rm FG}_{1234}\,|(12)_0(34)_0\rangle$$
$$-\exp[-\lambda(x_1-x_3)^2-\lambda(x_2-x_4)^2]\,f^{\rm FG}_{1324}\,|(13)_0(24)_0\rangle$$
$$+\exp[-\lambda(x_1-x_4)^2-\lambda(x_2-x_3)^2]\,f^{\rm FG}_{1423}\,|(14)_0(23)_0\rangle\,. \tag{3.12}$$

The notation $|(12)_0\rangle$ denotes the pairing of quarks 1 and 2 into a color singlet. The functions $f^{\rm FG}$ are the spatial wave functions appropriate for a Fermi gas. Upon putting the quarks in a box of length L and choosing antiperiodic boundary conditions, we have

$$f^{\rm FG}_{1234}\equiv\cos\frac{\pi}{L}(x_1+x_2-x_3-x_4)\,. \tag{3.13}$$

In $SU(2)_c$, two quarks can be put in a momentum state $+k$. The variational parameter λ describes the clustering of the quarks into hadrons. Equation (3.12) has several important properties.

(i) The wave function is explicitly antisymmetric under quark exchange.

(ii) The $\lambda=0$ wave function is equivalent to a Fermi gas Slater determinant.

(iii) The wave function separates into *color singlet* hadron clusters in the limit of large hadron-hadron separations, that is, for example, in the $|x_1-x_2|,|x_3-x_4|\to\infty$ limit.

The above wave function *Ansatz* can be readily generalized to N quarks. One starts by generating all distinct sets of quark pairs—in the case of four quarks, there are three such sets (12),(34), (13),(24), and (14),(23). One then determines the "symmetry" of each pairing with respect to one given pairing. That is, one counts the number of permutations, m, required to bring the pairing considered to the original pairing and then $(-1)^m$ determines whether that pairing is even or odd. That sign is the overall sign with which its contribution is added to the wave function. The contribution that a particular pairing $(12)(34)(56)(78)\cdots$ makes is $\exp[-\lambda(x^2_{12}+x^2_{34}+x^2_{56}+x^2_{78})]f^{\rm FG}(s_{12},s_{34},s_{56},s_{78}\ldots)$, where $x_{ij}\equiv x_i-x_j$ and $s_{ij}\equiv x_i+x_j$. The function $f^{\rm FG}$ is a symmetric function of its arguments, constructed from cosines of the $N/4$ momenta and all possible pairs of the s_{ij}'s. The allowed momenta in the box are odd multiples of π/L, as we choose to enforce antiperiodic boundary conditions. Thus, the function $f^{\rm FG}$ for the configuration 12345678... is

$$f^{\rm FG}_{12345678\ldots}=\sum_{P_h}\,{\rm per}\begin{vmatrix}\cos\frac{\pi}{L}(P^1_h-P^2_h) & \cos\frac{\pi}{L}(P^3_h-P^4_h) & \cdots\\ \cos\frac{3\pi}{L}(P^1_h-P^2_h) & \cos\frac{3\pi}{L}(P^3_h-P^4_h) & \cdots\\ \vdots & \vdots & \vdots\\ \cos(\frac{N}{2}-1)\frac{\pi}{L}(P^1_h-P^2_h) & \cos(\frac{N}{2}-1)\frac{\pi}{L}(P^3_h-P^4_h) & \cdots\end{vmatrix}\,. \tag{3.14}$$

Note that "per" denotes a permanent. A permanent is the symmetric version of a determinant, so that the various terms are just added together. In constructing the function $f^{\rm FG}_{12345678\ldots}$, we sum over all possible sets of distinct pairs of the hadronic coordinates s_{ij}, without regard to their order. A set of hadronic coordinates is itself labeled "P_h," and there are $(N/2)!/[2^{N/4}(N/4)!]$ different sets of distinct pairs for a given P_h. A member of P_h

is denoted by P_h^i. For a given P_h, we construct the permanent of the allowed momenta and the s_{ij} coordinates. In writing Eq. (3.14), we have assumed that the number of quarks is a multiple of 4. It is only in this case that the plane wave states for each free quark can be collapsed to an explicitly real wave function. Including the Fermi gas wave function is cumbersome, but it is absolutely necessary. In its absence, the variational procedure is not well posed, as the $\lambda = 0$ wave function is trivial.

In this manner, the total wave function can be constructed, and it satisfies all the points highlighted above for four quarks. Specifically, for eight quarks, we have

$$\begin{aligned}\Psi^{8q}_{\rm trial}(x_1,\ldots,x_8) = &\exp[-\lambda(x_{12}^2+x_{34}^2+x_{56}^2+x_{78}^2)]\; f^{\rm FG}_{12345678}\;|(12)_0(34)_0(56)_0(78)_0\rangle \\ &-\exp[-\lambda(x_{13}^2+x_{24}^2+x_{56}^2+x_{78}^2)]\; f^{\rm FG}_{13245678}\;|(13)_0(24)_0(56)_0(78)_0\rangle \\ &+\exp[-\lambda(x_{14}^2+x_{23}^2+x_{56}^2+x_{78}^2)]\; f^{\rm FG}_{14235678}\;|(14)_0(23)_0(56)_0(78)_0\rangle \\ &+\ldots(102\text{ terms})\,,\end{aligned} \tag{3.15}$$

where

$$\begin{aligned}f^{\rm FG}_{12345678} = &\cos\frac{\pi}{L}(s_{12}-s_{34})\cos\frac{3\pi}{L}(s_{56}-s_{78})+\cos\frac{3\pi}{L}(s_{12}-s_{34})\cos\frac{\pi}{L}(s_{56}-s_{78}) \\ &+\cos\frac{\pi}{L}(s_{12}-s_{56})\cos\frac{3\pi}{L}(s_{34}-s_{78})+\cos\frac{3\pi}{L}(s_{12}-s_{56})\cos\frac{\pi}{L}(s_{34}-s_{78}) \\ &+\cos\frac{\pi}{L}(s_{12}-s_{78})\cos\frac{3\pi}{L}(s_{34}-s_{56})+\cos\frac{3\pi}{L}(s_{12}-s_{78})\cos\frac{\pi}{L}(s_{34}-s_{56})\,.\end{aligned} \tag{3.16}$$

The difficulty with this procedure is that the number of distinct pairs of quarks grows greatly as N increases. There are $N!/[2^{N/2}(N/2)!]$ terms in the N quark wave function, so that the calculation quickly becomes unmanageable. There are 105 terms in the eight quark wave function, but there are 10 395 terms in the twelve quark wave function.

Enumerating all the exchange terms by brute force is not practical, nor is it necessary. Our interest is not in the wave function itself, but, rather, in the observables associated with it. We are interested in the matrix elements $\langle\Psi|\hat{O}|\Psi\rangle$, where $\hat{O}$ is a symmetric—and color-independent—operator. For example, $\hat{O}=\hat{T}=-\frac{1}{2}\sum_j\partial_j^2$; $\hat{O}$ can be the kinetic energy operator. *It turns out that permutation symmetry greatly reduces the number of nontrivial terms.* Consequently, for eight quarks, say, the matrix element of the symmetric operator $\hat{O}$ can be written

$$\begin{aligned}\langle\Psi^{8q}_{\rm trial}|\hat{O}|\Psi^{8q}_{\rm trial}\rangle \propto \int dx_i f_{12345678}\;\hat{O}\;\Big[&(1)f_{12345678}-(12)\frac{1}{2}f_{14325678} \\ &+(32)\frac{1}{4}f_{14365278}+(12)\frac{1}{4}f_{14325876}-(48)\frac{1}{8}f_{14365872}\Big]\,,\end{aligned} \tag{3.17}$$

where $f_{12345678}\equiv f^{\rm FG}_{12345678}\;\exp[-\lambda(x_{12}^2+x_{34}^2+x_{56}^2+x_{78}^2)]$. For the matrix elements of an operator $\hat{O}$ of the type above, one need only count occurrences of topologically distinct terms. These are terms which cannot be brought into each other under rotation of the coordinate indices. For example, for eight quarks, starting with 12 34 56 78, there are

"singles" $\leftrightarrow$ 14 32 56 78$\leftrightarrow$ "[1]"
"doubles" $\leftrightarrow$ 14 36 52 78$\leftrightarrow$ "[2]"
"triples" $\leftrightarrow$ 14 36 58 72$\leftrightarrow$ "[3]"

and

"disconnected doubles" $\leftrightarrow$ 14 32 58 76 $\leftrightarrow$ "[1+1]".

The terms in brackets have been introduced as a convenient notation, so that we can extend this construction to N quarks. We use "singles" or "[1]" to denote the single exchange of quarks between two clusters, whereas "doubles" or "[2]" denotes the exchange of quarks between three clusters such that one quark in the first cluster ends up in the third. This is in contrast to a "[1+1]" exchange, in which two single exchanges occur between two separate pairs of clusters. In Eq. (3.17), the numbers in parentheses are the number of terms of that type in the original wave function, so that their sum is 105. The fractions are the color matrix elements for terms of that type, note that $\langle(12)_0(34)_0(56)_0\ldots|(12)_0(34)_0(56)_0\ldots\rangle = 1$, so that, for example, $\langle(12)_0(34)_0|(14)_0(32)_0\rangle = 1/2$. Since we do compute the color matrix element, we need only consider permutations of one member of a particular pair of quarks; in the above, for example, we have kept the odd quarks fixed and considered exchanges of the even ones. The sum of all the coefficients, then, including the color matrix element, is $(N/2)!$, or 24 for the

eight quark case.

For N quarks, one can write the general form of the coefficient, given its topological structure. Moreover, one can enumerate all the possible topological structures for a fixed number of quarks. In order to discuss this, we shall use the "$[i+j+k+\cdots]$" notation defined above.

The distinct topological terms for a fixed number of quarks are given by $[i+j+k+\cdots]$, where the range of $i,j,k,\ldots$ satisfies the following bounds. That is, i ranges from 1 to the upper bound $\xi = N/2-1$ and $j,k,\ldots$ range from 0 to ξ, subject to the constraints that $i+j+k+\cdots(\kappa \text{ terms}) \leq \xi-\kappa+1$ and $i \leq j \leq k \leq \ldots$ when $j,k,\ldots \neq 0$. For eight quarks, the terms are [1], [2], [3], [1 + 1]. For twelve quarks, the terms are [1], [2], [3], [4], [5], [1 + 1], [1 + 2], [1 + 3], [2 + 2], [1 + 1 + 1]. The formula for the overall coefficient of the $[i+j+k+\cdots]$ term can be expressed in closed form. That is

$$C_{[i+j+k+\cdots]} = \frac{1}{s}\left[\frac{(-1)^{i+j+k+\cdots}}{(i+1)(j+1)(k+1)\cdots}\right] \times (n_H)\cdots(n_H-i-j-k)\,, \tag{3.18}$$

where $n_H \equiv N/2$, and s is a symmetry factor. s is determined by the number of repeated exchanges. That is, if $[i+j+k+\cdots]$ has I terms of type i and J terms of type j, and all the other terms are distinct, then $s = I!\,J!$. For example, with $[1+1]$, $s = 2$. Thus, we have a strategy for the computation of the $\langle\Psi^{Nq}_{\text{trial}}|\hat{O}|\Psi^{Nq}_{\text{trial}}\rangle$ matrix element:

$$\langle\Psi^{Nq}_{\text{trial}}|\hat{O}|\Psi^{Nq}_{\text{trial}}\rangle \propto \int\{dx_i\} f_{1234\cdots N} O \Psi^{Nq}_{\text{trick}} \tag{3.19}$$

where

$$\Psi^{Nq}_{\text{trick}} = f_{1234\cdots N} + {\sum_{i,j,k,\ldots}}' C_{[i+j+k+\cdots]} f_{[i+j+k+\cdots]}\,. \tag{3.20}$$

The notation $\sum'$ means that the sum is restricted. As above, we require that $i \leq j \leq k \ldots$ when $j,k,\ldots \neq 0$ and $i+j+k+\cdots(\kappa \text{ terms}) \leq N/2-\kappa$. Note that i starts at one, whereas $j,k,\ldots$ begin at zero. In Sec. V, we discuss the stochastic evaluation of Eq. (3.19) and the resulting computation of the total energy and the two-body correlation function with density.

We can compute the $\langle\Psi^{Nq}_{\text{trial}}|\hat{O}|\Psi^{Nq}_{\text{trial}}\rangle$ matrix element in another manner. That is,

$$\langle\Psi^{Nq}_{\text{trial}}|\hat{O}|\Psi^{Nq}_{\text{trial}}\rangle \propto \int\{dx_i\}\left(\Psi^{Nq}_{\text{trial}}\right)_{\uparrow\downarrow\uparrow\downarrow\ldots} O \left(\Psi^{Nq}_{\text{trial}}\right)_{\uparrow\downarrow\uparrow\downarrow\ldots}\,. \tag{3.21}$$

Here "↑" and "↓" denote the two color states of the model, and $(\Psi^{Nq}_{\text{trial}})_{\uparrow\downarrow\uparrow\downarrow\ldots}$ denotes a projection of the full wave function on the $\langle\uparrow\downarrow\uparrow\downarrow\ \ldots|$ state. We have written the integrand in Eq. (3.21) as a manifestly positive definite quantity. This is highly convenient for a stochastic evaluation of the integral, though it is at the cost of a more complicated wave function. This wave function contains $(N/2)!$ terms, but it is simply related to Ψ^{Nq}_{trick}. Starting with Ψ^{Nq}_{trick}, we enumerate all the terms of a particular topological class. Thus, for eight quarks, in place of the term with

$$[1] \leftrightarrow 14\ 32\ 56\ 78 \tag{3.22}$$

we explicitly include all 6 terms of that type. That is,

14 32 56 78
16 34 52 78
18 34 56 72
12 36 54 78
12 38 56 74
12 34 58 76.

In this manner, $(\Psi^{Nq}_{\text{trial}})_{\uparrow\downarrow\uparrow\downarrow\ldots}$ can be readily generated.

We shall study the benefits and disadvantages offered by Eq. (3.19) and Eq. (3.21) in Sec. V.

IV. COMPARISON WITH OTHER MODELS

Here we compare the model defined by Eq. (3.12) with previous attempts to incorporate SU(N) color. To our knowledge, our model study is the first complete treatment of SU(2)$_c$ in quark matter. To make our treatment of hidden color forces clear, we first consider the original SU(N)$_c$ study of Lenz *et al.* [4] in the $q^2\bar{q}^2$ system. For a particular pairing (12)(34), for example, they postulate that confining forces of differing range may reside in the orthogonal sectors $|(12)_0(34)_0\rangle$ and $|(12)_1(34)_1\rangle_0$. The sector in which the individual quarks are paired to triplets before being paired to an overall singlet is the "hidden color" sector.

The color kets of Eq. (3.12) can be recast into the framework described above. That is, the kets $|(13)_0(24)_0\rangle$ and $|(14)_0(23)_0\rangle$ can be expressed as linear combinations of $|(12)_0(34)_0\rangle$ and $|(12)_1(34)_1\rangle_0$. Following Lenz *et al.* [4], we introduce the coordinates

$$\begin{aligned} x &= \frac{1}{2}(x_1+x_3-x_2-x_4), \\ y &= \frac{1}{2}(x_1+x_2-x_3-x_4), \\ z &= \frac{1}{2}(x_1+x_4-x_3-x_2)\,. \end{aligned} \tag{4.1}$$

These are useful reduced variables, as they describe the relative separation of hadrons with a particular quark content. With Eq. (4.1), we can rewrite Eq. (3.12) as

$$\Psi^{4q}_{\rm trial} = \left[\exp[-2\lambda(x^2+z^2)]\, f^{\rm FG}_{1234} - \frac{1}{2}\exp[-2\lambda(y^2+z^2)]\, f^{\rm FG}_{1324} - \frac{1}{2}\exp[-2\lambda(x^2+y^2)]\, f^{\rm FG}_{1423} \right] |(12)_0(34)_0\rangle$$
$$+ \left[-\frac{1}{2}\exp[-2\lambda(y^2+z^2)]\, f^{\rm FG}_{1324} + \frac{1}{2}\exp[-2\lambda(x^2+y^2)]\, f^{\rm FG}_{1423} \right] |(12)_1(34)_1\rangle_0 \tag{4.2}$$

where

$$|(12)_1(34)_1\rangle_0 \equiv (|(12)\ 11\rangle|(34)\ 1\text{-}1\rangle + |(12)\ 1\text{-}1\rangle|(34)\ 11\rangle - |(12)\ 10\rangle|(34)\ 10\rangle)/\sqrt{3}.$$

Note that in $|(12)\ {\rm IJ}\rangle$ I and J denote the z component of the color of quarks 1 and 2, respectively. We see manifestly, then, that hidden color states are equivalent to the coupling of the other pairs of quarks to singlets, and, thus, are trivial. Indeed, in the absence of active gluon degrees of freedom, this is generally so. In the channel with the pairing (12)(34), the relative separation of (12) and (34) is determined by y—so it is the "channel" variable. The exchange terms in the color singlet and hidden color sectors have the same behavior in y, so that the spatial range of the confining forces in the two sectors is the same. Lenz *et al.* [4] considered the $q^2\bar{q}^2$ system in three spatial dimensions as a function of a parameter specifying the relative spatial range of the color singlet (comprised of color singlets) and hidden color sectors. Our model of hidden color forces maps to one particular case in their study, although there is no special physics reason for our choice.

The full SU(2) treatment of Sec. III can also be compared with the approximate treatment of Horowitz and Piekarewicz [7]. Their work was in SU(3) color and three spatial dimensions; we now consider this approach in $SU(2)_c$ for purposes of comparison. In their treatment of color, the quarks are given *fixed* colors. (Watson [8] has also used this starting point.) For this reason, in the discussions to come, we will refer to this approach as the "painted" model. In constrast to Eq. (2.3), the potential is no longer color blind, but, rather, consists of the minimum energy pairing of quarks of differing color. The construction of a totally antisymmetric, color singlet variational *Ansatz* is straightforward. That is,

$$\Psi^{Nq}_{\rm trial} = \exp[-\lambda \hat{V}_{\rm RB}]\ \Psi^{\rm FG}_{\rm R}\Psi^{\rm FG}_{\rm B}\ , \tag{4.3}$$

where

$$\hat{V}_{\rm RB} = \min_{[L,M]} \sum_{i,j=1}^{N/2} v(x^r_{L^i} - x^b_{M^j}) \tag{4.4}$$

such that $v(x^r_{L^1} - x^b_{M^1}) = (x^r_{L^1} - x^b_{M^1})^2/2$. The L and M are elements of the permutation group $S_{(N/2)}$, and L^i is the ith member of the element L. We have presumed that there are equal numbers of red (R) and blue (B) quarks and that their coordinates are labeled by the appropriate superscripts. Note that $\Psi^{\rm FG}_{\rm R}$ is the Slater determinant for the red quarks. The following convenient form is equivalent to a Slater determinant:

$$\Psi^{\rm FG}_{\rm R} = \prod_{n,m\ {\rm odd}}^{N} \sin\left[\frac{\pi}{L}(x_n - x_m)\right]\ . \tag{4.5}$$

This method is simple to implement and is able to treat many quarks with ease. We will compare the full $SU(2)_c$ results to the simple approximation described here for two reasons. First, we wish to examine the extent to which the predictions of the painted model are robust. Its primary advantage is convenience; we cannot expect the painted model to be exact as all color flipping transitions, i.e., RB $\leftrightarrow$ BR, are neglected. However, the differences might not be large. Second, we hope that any departures between the full $SU(2)_c$ and painted calculations will give us greater insight into the nature of the correlations in the full calculation.

We can begin to understand the difference between the painted [approximate $SU(2)_c$] and magic [full $SU(2)_c$] models through consideration of their variational *Ansätze* for four quarks. That is, for the magic model,

$$\begin{aligned}\langle\uparrow\downarrow\uparrow\downarrow|\Psi^{4q}_{\rm M}\rangle = {} & \exp\left[-\lambda[(x_1-x_2)^2+(x_3-x_4)^2]\right] \\ & \times\cos\frac{\pi}{L}(x_1+x_2-x_3-x_4) \\ & -\exp\left[-\lambda[(x_1-x_4)^2+(x_2-x_3)^2]\right] \\ & \times\cos\frac{\pi}{L}(x_1+x_4-x_2-x_3)\end{aligned} \tag{4.6}$$

whereas, in the painted model,

$$\begin{aligned}\langle\uparrow\downarrow\uparrow\downarrow|\Psi^{4q}_{\rm P}\rangle = {} & \exp\left[-\lambda\min[V_{(12),(34)}, V_{(14),(23)}]\right] \\ & \times\sin\frac{\pi}{L}(x_1-x_3)\sin\frac{\pi}{L}(x_2-x_4)\end{aligned} \tag{4.7}$$

where quarks 1,3 are red ("up") and quarks 2,4 are blue ("down"). The Hamiltonians of the two models differ, but it is still useful to compare the structure of the *Ansätze* as two quarks of the same color approach each other. In this way, we can understand more about the dynamical content of the two models. Letting $x_1 - x_3 \equiv \varepsilon$ be small, we have

$$\begin{aligned}\langle\uparrow\downarrow\uparrow\downarrow|\Psi^{4q}_{\rm M}\rangle = {} & \exp\left[-\lambda[(x_2-x_3)^2+(x_3-x_4)^2]\right] \\ & \times\{-2\varepsilon\frac{\pi}{L}\sin\frac{\pi}{L}(x_2-x_4) \\ & +2\lambda(x_2-x_4)\varepsilon\cos\frac{\pi}{L}(x_2-x_4)+O(\varepsilon^2)\}\end{aligned} \tag{4.8}$$

for the full $SU(2)_c$ calculation and

$$\langle\uparrow\downarrow\uparrow\downarrow|\Psi_{\rm P}^{4q}\rangle = \exp\left[-\lambda[(x_2-x_3)^2+(x_3-x_4)^2]\right] \times\left\{\varepsilon\frac{\pi}{L}\sin\frac{\pi}{L}(x_2-x_4)+O(\varepsilon^2)\right\} \quad (4.9)$$

for the painted model. Equation (4.8) contains an additional term in leading order in ε. This term does not have the same manifest L dependence as the term which both Eqs. (4.8) and (4.9) share. Indeed, this additional term suggests that the Fermi "wound" should heal more quickly in the full SU(2)$_c$ calculation than in the painted case, even for large L. This qualitative difference in the structure of the *Ansätze* will be manifest in a comparison of the models' two-body densities.

V. MONTE CARLO COMPUTATIONS

In this section, we shall discuss the techniques necessary to evaluate the integrals in Eq. (3.19) and Eq. (3.21), so that the total energy of the system and its two-body density may be computed. First, we shall discuss the computation of the system's energy. Let us consider, then, the evaluation of the kinetic energy: $T=-(1/2)\sum_i\partial_i^2$. Both Eq. (3.19) and Eq. (3.21) have terms purely of the form

$$f^{\lambda}_{12345678\ldots}f^{\rm FG}_{12345678\ldots}\,, \quad (5.1)$$

where

$$f^{\lambda}_{12345678\ldots}=\exp\{-\lambda[(x_1-x_2)^2+(x_3-x_4)^2+(x_5-x_6)^2+(x_7-x_8)^2+\cdots]\} \quad (5.2)$$

and $f^{\rm FG}_{12345678\ldots}$ has been introduced in Eq. (3.14). For wave functions of this structure, the kinetic energy can be calculated in a straightforward way. Note that

$$\partial_1 f^{\rm FG}_{1234\ldots}=\partial_2 f^{\rm FG}_{1234\ldots} \quad (5.3a)$$

whereas

$$\partial_1 f^{\lambda}_{1234\ldots}=-\partial_2 f^{\lambda}_{1234\ldots}\,, \quad (5.3b)$$

so that $\sum_{i=1}^{2}\partial_i f^{\lambda}_{1234\ldots}\partial_i f^{\rm FG}_{1234\ldots}=0$. This cancellation occurs pairwise, so that

$$-\frac{1}{2}\sum_{j=1}^{N}\partial_j^2(f^{\lambda}_{1234\ldots}f^{\rm FG}_{1234\ldots})=-\frac{1}{2}\sum_{j=1}^{N}[(\partial_j^2 f^{\lambda}_{1234\ldots})f^{\rm FG}_{1234\ldots}+f^{\lambda}_{1234\ldots}(\partial_j^2 f^{\rm FG}_{1234\ldots})] \quad (5.4a)$$

$$=[\lambda N-4\lambda^2(x_1-x_2)^2+(x_3-x_4)^2+\cdots]f^{\lambda}_{1234\ldots}f^{\rm FG}_{1234\ldots}+t_{\rm FG}Nf^{\lambda}_{1234\ldots}f^{\rm FG}_{1234\ldots}. \quad (5.4b)$$

Note that $t_{\rm FG}$ is the Fermi gas kinetic energy per quark for a finite number of quarks. Upon choosing antiperiodic boundary conditions, the allowed momenta in the box are odd integers, and

$$t_{\rm FG}^{\rm a-p}=\frac{2\pi^2}{NL^2}\sum_{i=1}^{N/4}(2i-1)^2\,, \quad (5.5)$$

so that

$$t_{\rm FG}^{\rm a-p}=\frac{\pi^2\rho^2}{24}\left(1-\frac{4}{N^2}\right)\,, \quad (5.6)$$

where the density $\rho=N/L$ has been introduced. For large N, this is the continuum SU(2) Fermi gas kinetic energy; the corrections to this limit are of order $1/N^2$. We hope that this effect will persist for other observables and for finite λ.

With the use of Eq. (5.4b) and Eq. (5.6), the form of the derivative terms can be realized analytically. We are able, then, to write down the precise form of the matrix elements we wish to calculate. Presuming that the initial matrix element is of the form given in Eq. (3.21) and letting $\tilde{A}\equiv(\Psi_{\rm trial}^{Nq})_{\uparrow\downarrow\uparrow\downarrow\ldots}$, the kinetic energy per particle $\langle t\rangle_\lambda$ and the potential energy per particle $\langle v\rangle_\lambda$ become

$$\langle t\rangle_\lambda=t_{\rm FG}+\lambda-\frac{4\lambda^2}{N}\frac{\int\{dx_i\}\tilde{A}\tilde{g}}{\int\{dx_i\}\tilde{A}^2} \quad (5.7)$$

and

$$\langle v\rangle_\lambda=\frac{1}{N}\frac{\int\{dx_i\}\tilde{A}V\tilde{A}}{\int\{dx_i\}\tilde{A}^2}\,, \quad (5.8)$$

where

$$\tilde{g}\equiv[(x_1-x_2)^2+(x_3-x_4)^2+(x_5-x_6)^2+(x_7-x_8)^2+\cdots]f_{12345678\ldots} -[(x_1-x_4)^2+(x_3-x_2)^2+(x_5-x_6)^2+(x_7-x_8)^2+\cdots]f_{14325678\ldots}+\ ((N/2)!-2)\ \text{terms}, \quad (5.9)$$

and V denotes the usual many-body potential, Eq. (2.3). Note that the total energy per particle is $\langle\varepsilon\rangle_\lambda=\langle t\rangle_\lambda+\langle v\rangle_\lambda$. The numerator of Eq. (5.7) no longer has a $\tilde{A}^2$ structure; indeed we "measure" $\tilde{g}/\tilde{A}$ with respect to the distribution $\tilde{A}^2$. Note that configurations with $\tilde{A}=0$ are generated with zero weight, so that the procedure we effect actually works rather well.

Before we proceed, we should mention how the potential, Eq. (2.3), is calculated. The economics literature [24] abounds with numerical algorithms for minimization

problems—we need only recall the "traveling salesman" problem. For our purposes, determining the optimum pairing in one spatial dimension is simple. The continuous system is modeled by quarks on a ring; a particular quark on that ring can be paired with its neighbor to its left or its right, and that one choice determines the partners for all the other quarks on the ring. Thus, we only have to calculate the energy of the two different arrangements to determine the optimum pairing. Clearly, any arrangement which involves overlapping strings cannot be an optimum pairing.

Our results depend on the variational parameter λ, and we wish to determine the optimal λ in an efficient way. We must find λ_t such that

$$\frac{d}{d\lambda}\langle\varepsilon\rangle_\lambda\bigg|_{\lambda=\lambda_t} = 0 \,. \tag{5.10}$$

We can do this by exploiting how the matrix elements scale in λ and L. The wave function *Ansatz* itself is a function of the dimensionless variable λL^2 alone, but the final matrix elements do have a manifest L dependence. That is,

$$\langle t\rangle_\lambda \sim \left[\frac{1}{L^2}\right], \tag{5.11a}$$

$$\langle v\rangle_\lambda \sim \left[L^2\right] . \tag{5.11b}$$

The dependence of the t and v matrix elements on L differ, so that the optimal L—and, hence, the optimal λ—can be computed directly from $d\langle t\rangle_\lambda/d\lambda$ and $d\langle v\rangle_\lambda/d\lambda$. In this way, a single calculation for fixed λL^2 suffices to determine the optimal variational parameter and the observables for that λ. We calculate $d\langle t\rangle_\lambda/d\lambda$ and $d\langle v\rangle_\lambda/d\lambda$ directly, as computing the numerical derivative in λ of the stochastically calculated t and v matrix elements is unwieldy. Moreover, sampling the appropriate derivatives directly does not require much additional effort. Thus, we compute

$$\frac{d}{d\lambda}\langle t\rangle_\lambda = 1 - \frac{8\lambda}{N}\frac{\int\{dx_i\}\tilde{A}\tilde{g}}{\int\{dx_i\}\tilde{A}^2} + \frac{4\lambda^2}{N}\frac{\int\{dx_i\}(\tilde{A}\tilde{h}+\tilde{g}^2)}{\int\{dx_i\}\tilde{A}^2} - \frac{8\lambda^2}{N}\left[\frac{\int\{dx_i\}\tilde{A}\tilde{g}}{\int\{dx_i\}\tilde{A}^2}\right]^2 \tag{5.12}$$

and

$$\frac{d}{d\lambda}\langle v\rangle_\lambda = -\frac{2}{N}\frac{\int\{dx_i\}\tilde{A}V\tilde{g}}{\int\{dx_i\}\tilde{A}^2} + \frac{2}{N}\frac{\int\{dx_i\}\tilde{A}\tilde{g}\int\{dx_i\}\tilde{A}V\tilde{A}}{\left[\int\{dx_i\}\tilde{A}^2\right]^2} , \tag{5.13}$$

where $\tilde{g}$ is given by Eq. (5.9) and

$$\tilde{h} \equiv [(x_1-x_2)^2+(x_3-x_4)^2+(x_5-x_6)^2+(x_7-x_8)^2+\cdots]^2 f_{12345678\ldots} - [(x_1-x_4)^2+(x_3-x_2)^2+(x_5-x_6)^2+(x_7-x_8)^2+\cdots]^2 f_{14325678\ldots} + ((N/2)!-2)\text{ terms} . \tag{5.14}$$

As in Eq. (5.7), we measure $\tilde{g}/\tilde{A}$, as well as $\tilde{h}/\tilde{A}$ and $(\tilde{g}/\tilde{A})^2$, with respect to the distribution $\tilde{A}^2$. We can now proceed to construct the optimal variational solution for some fixed λL^2. We shall label the observables computed at some ρ_0 and λ_0 by "0," and the observables at the desired scaled point by "t," That is, we want ρ_t and λ_t such that

$$\frac{d\langle t\rangle_t}{d\lambda} + \frac{d\langle v\rangle_t}{d\lambda} = 0 \,, \tag{5.15}$$

so that

$$\frac{d\langle t\rangle_0}{d\lambda} + \left[\frac{\rho_0}{\rho_t}\right]^4 \frac{d\langle v\rangle_0}{d\lambda} = 0 \,. \tag{5.16}$$

Thus, the optimal L—or, rather, ρ_t—for fixed λL^2 is given by

$$\rho_t = \rho_0 \left[\frac{-d\langle t\rangle_0/d\lambda}{d\langle v\rangle_0/d\lambda}\right]^{-1/4} . \tag{5.17}$$

Introducing

$$\eta = \left[\frac{\rho_0}{\rho_t}\right]^2 , \tag{5.18}$$

we can compute the optimum λ

$$\lambda_t = \frac{\lambda_0}{\eta} , \tag{5.19}$$

as well as the kinetic and potential energies at the new point

$$\langle t\rangle_t = \frac{\langle t\rangle_0}{\eta} \tag{5.20}$$

and

$$\langle v\rangle_t = \eta\langle v\rangle_0 . \tag{5.21}$$

Of course, $\langle\varepsilon\rangle_t = \langle t\rangle_t + \langle v\rangle_t$. These scaling relations serve to generate the optimal variational solution for some fixed λL^2. Their utility depends on the energy having a smooth, parabolic behavior in the region of λ_t, ρ_t. Even if this constraint is satisfied, as it is here, we cannot strictly say that we have determined the best variational solution for a fixed density. For a fixed density, there exist two separate parametric families—those with finite λ and those with $\lambda = 0$. Scaling relations also exist for the $\lambda = 0$ family. The $\lambda = 0$ solution may have a lower energy than the finite λ solution for some fixed density; the relative energies of the two families must be determined

"empirically."

In principle, we have two distinct strategies, Eqs. (3.19) and (3.21), for computing the observables associated with the Hamiltonian of Eqs. (2.2) and (2.3). The wave function in Eq. (3.19) is much simpler, but we must compute its normalization explicitly. We have compared the two schemes for both eight and twelve quarks, and have found Eq. (3.21) to be the method of choice. The two strategies do yield identical results within error bars, as they should, but *many* more integration points are required to yield good results in the case where we must calculate the normalization. Consequently, the formulas and results we present exploit Eq. (3.21).

Thus far, we have described the procedure by which the optimal variational calculation of the energy is effected. However, we are interested in more than the energetics of the system; we would also like to study the structure of the ground state. We are particularly interested in the correlations induced in the ground state as a result of the internal color degree of freedom and global antisymmetry. Thus, we shall now describe how the two-body density may be calculated as well. The two-body density operator, $\hat{\rho}_2(r)$, is defined as

$$\hat{\rho}_2(r) = \frac{1}{L}\sum_{i\neq j}\delta(r-(x_i-x_j)) \; . \tag{5.22}$$

This operator is manifestly symmetric, so that we may compute the resulting matrix element in the manner indicated by Eq. (3.21). We choose to normalize the matrix element of the two-body density by the square of the one-body density; that is, we shall compute the matrix element of $\hat{\rho}_2(r)/\rho_0^2$. With this choice of normalization, the low-density limit of this matrix element is

$$\frac{\langle\rho_2(r)\rangle_{\rho_0\to 0}}{\rho_0^2} = \frac{|\Psi_{\rm isol}(r)|^2}{\rho_0} \; . \tag{5.23}$$

$|\Psi_{\rm isol}(r)|^2$ is the square of the isolated hadron wave function; here

$$|\Psi_{\rm isol}(r)|^2 = \left(\frac{1}{\sqrt{2}\pi}\right)^{1/2} e^{-\sqrt{2}r^2/2} \; , \tag{5.24}$$

so that the low density limit of the clustering parameter λ is

$$\lambda(\rho\to 0) = \frac{1}{2\sqrt{2}} \simeq 0.35 \; . \tag{5.25}$$

The matrix element of Eq. (5.22) measures the correlation of any two quarks as a function of their separation r in the system's ground state. At low densities, the quark-quark correlation function is controlled by the isolated hadron wave function, as shown in Eq. (5.23). At high densities, the system becomes a nonrelativistic Fermi gas. In this limit, the two-body density is

$$\frac{\langle\rho_2(r)\rangle_{\rm FG}}{\rho_0^2} = 1 - \frac{1}{2}j_0^2(k_F r) \; , \tag{5.26}$$

where, in SU(2)$_c$, the Fermi momentum k_F is given by $k_F = \pi\rho_0/2$. There is a 50% probability that any two quarks in SU(2)$_c$ will have different color states; hence, the two-body density at $r = 0$ is 1/2.

The Metropolis Monte Carlo procedure we use allows us to calculate the two-body density in a straightforward way. That is, we generate the quarks' coordinates according to the distribution $|(\Psi_{\rm trial}^{Nq})_{\uparrow\downarrow\uparrow\downarrow\ldots}|^2$, in order to calculate matrix elements according to Eq. (3.21). We can compute the matrix element of Eq. (5.22) with r by simply tabulating the occurrences of $x_i - x_j$ in the generated distribution over the interval $[0, L]$ in bins of Δr. The resulting histogram is a discrete representation of the two-body density with r. As in the case with the energy, scaling can be used to calculate the two-body density for the optimum value of the variational parameter at some fixed density in an economical manner. The quantity $\langle\rho_2(r)\rangle_{\rho_0\to 0}/\rho_0^2$ is itself L independent, but the scale in r over which it is plotted does depend on L. The stepsize in r upon scaling from ρ_0 to ρ_t transforms according to

$$(\Delta r)_t = (\Delta r)_0\left(\frac{\rho_0}{\rho_t}\right) \; . \tag{5.27}$$

In this manner, the two-body density at the scaled values of the density and variational parameter can be computed from some initial ρ_0 and λ_0.

VI. RESULTS

In this section, we shall present our variational Monte Carlo results, computed using Eq. (3.21). We have computed the energy and correlation function as a function of density for eight and twelve quarks. The low and high density limits of the model are known exactly, so that it is useful to review those results before proceeding to a discussion of the simulations. At low densities, the energy per quark ε and the variational parameter λ are given by the isolated hadron values. The isolated hadron wave function in our units is given by Eq. (5.24), so that at low densities,

$$\langle\varepsilon\rangle_\lambda \to \frac{1}{2\sqrt{2}} \simeq 0.35 \tag{6.1a}$$

$$\langle t\rangle_\lambda \to \langle v\rangle_\lambda \to \frac{\langle\varepsilon\rangle_\lambda}{2} \simeq 0.18 \; . \tag{6.1b}$$

Equation (6.1b) is a consequence of the virial theorem in the isolated hadron limit. The isolated hadron variational parameter is given in Eq. (5.25).

We shall first examine the energy and variational parameter as a function of density before turning to the correlation function results.

A. Energy vs density

Figure 2 shows the variational parameter λ as a function of density for eight quarks. The indicated points are the lowest energy solutions as a function of density for the finite λ parametric family. At low density, the scal-

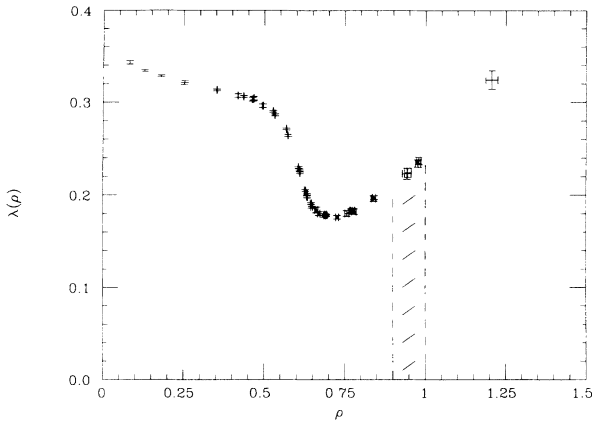

FIG. 2. The variational parameter λ as a function of ρ for eight quarks. The points indicate the optimum finite λ solutions as a function of density, and the associated error bars are indicated. The hatched region indicates a transition region from finite to zero λ, and its width is 2σ, where sigma is the error assigned to the transition density estimate.

ing solution approaches the isolated hadron limit value, Eq. (5.25). At high density, the energies of the optimal solutions of the finite λ and zero λ families cross; the variational parameter drops to zero for $\rho \sim 1$. The manner in which this level crossing occurs is shown in Fig. 3. At low density, the energy as a function of the variational parameter has a single extremum. As the density increases, a double-welled structure develops; at sufficiently high density, the zero λ solution is lower in energy. The two extrema are well separated in λ; this generates the sudden drop in λ with ρ seen in Fig. 2. This behavior is a nontrivial dynamical consequence of the model.

The meaning of "high" density is not yet clear, as the scale in Fig. 2 is in dimensionless units. In the units of this paper, the rms separation of the quarks in an isolated ground state hadron [noting Eqs. (5.24) and (5.25)] is

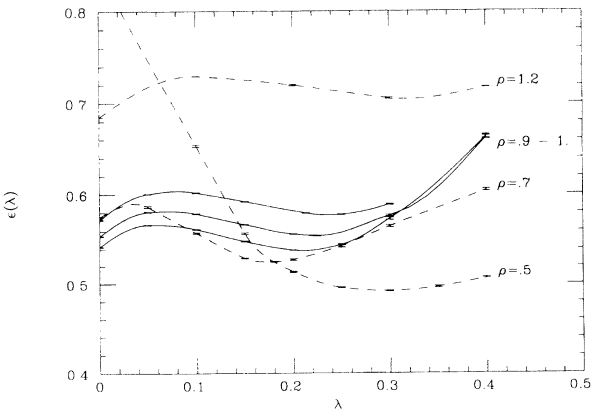

FIG. 3. The energy per particle $\varepsilon(\lambda)$ as a function of λ for various, fixed ρ. The lines are merely to guide the eye. The solid lines are $\varepsilon(\lambda)$ vs λ in the transition region to zero λ; the densities for those curves from bottom to top are 0.90, 0.95, and 1.0, respectively.

$$\langle r^2 \rangle^{\frac{1}{2}} = \frac{1}{2\sqrt{\lambda_{\rm isol}}} \simeq 0.84 \qquad (6.2)$$

so that one hadron in an isolated hadron length implies a quark number density of 2.4. The number density of realistic nuclear matter at saturation is 0.17 fm^{-3}. The charge radius of the proton in the nonrelativistic quark model [25] is 0.5 fm, so that putting one proton in the volume given by that radius corresponds to a number density of 1.9 fm^{-3}. Consequently, the density 0.95 in our units corresponds roughly to 4 times nuclear matter density, although one must be cautious in assigning dimensions in this simple model.

Figure 4 shows the energy per particle of the eight quark system for the optimum variational parameters of Fig. 2. The energies of the finite λ and zero λ solutions are plotted in the same figure. As previously illustrated in Fig. 3, the energies of the finite and zero λ solutions cross at $\rho \sim 1$. As the density increases, the potential energy goes to zero. In that limit, the total energy per particle is that of a free Fermi gas. This is natural—the interquark separation, and, hence, the string length, approaches zero as $\rho \to \infty$. At low densities, the total energy per particle approaches the isolated hadron value, and the virial theorem ($t = v$) appears to be satisfied in that limit as well. Note that nuclear matter in this eight quark calculation, at least, is not bound. At moderate densities, a dynamical interplay exists between the potential and kinetic energies. That is, for a slightly larger average string length, the shape of the spatial wave function can "relax" and reduce its kinetic energy.

We shall now consider the variational parameter λ and the energy per particle as a function of density for twelve quarks, as we would like to see how sensitive our results

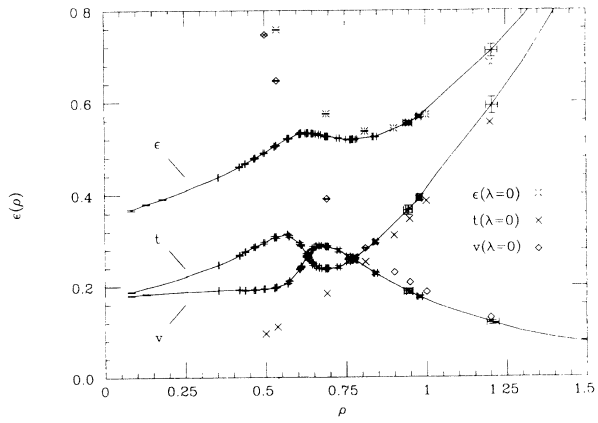

FIG. 4. The total energy per particle $\varepsilon(\rho)$ as a function of ρ for eight quarks. The kinetic energy per particle is denoted by "t," whereas the potential energy per particle is denoted by "v." The lines are merely to guide the eye. The points connected by lines are the energies associated with the finite λ variational solution. The energies ε, t, and v associated with the zero λ solution are plotted as well; the symbol definitions are indicated in the figure. The error bars associated with these points are plotted, when they are large enough to be visible. The $t(\lambda = 0)$ points correspond to a free Fermi gas, so that there are no associated errors.

are to finite size effects. Figure 5 shows the twelve quark results for the optimal variational parameter λ as a function of ρ. The eight quark results from Fig. 2 are plotted as well for comparison. The twelve quark calculation approaches the isolated hadron limit as $\rho \to 0$, and it undergoes a transition to zero λ in the same region of ρ. However, the results at intermediate density are different. The optimum variational parameter in the twelve quark case decreases more quickly as the system moves away from the isolated hadron limit, although it does not have the dip at $\rho \sim 0.75$ that exists in the eight quark case. If we now turn to the energy per particle as a function of density, we see the finite size effects are substantial there as well. These results are shown in Fig. 6. The energy per particle for the twelve quark case obeys the high and low density limits of the model: the system evolves to the isolated hadron energy per particle and to equal t and v as the density goes to zero, and it approaches the Fermi gas limit as the density goes to infinity. Figure 6 also shows the level crossing behavior of the finite and zero λ families seen in Fig. 4 and inferred from Fig. 5. The "softening" of λ seen in the twelve quark case at $\rho \sim 0.3$ is reflected in the slower increase in t in that density regime. The consequence is that the energy per particle skims along at the isolated hadron energy per particle for a nontrivial interval in ρ before finally increasing. This is in contrast to the eight quark case, where ε increases steadily as a function of density. Neither the eight nor twelve quark case supports a bound state; yet, the change in ε in going from eight to twelve quarks in the $\rho \sim 0.3$ regime suggests that a bound state cannot be ruled out in this model as the number of quarks goes to infinity. The finite size effects are still larger in the $\rho \sim 0.75$ regime. There, the interplay between t and v seen in the eight quark case is simply absent. This is entirely consistent

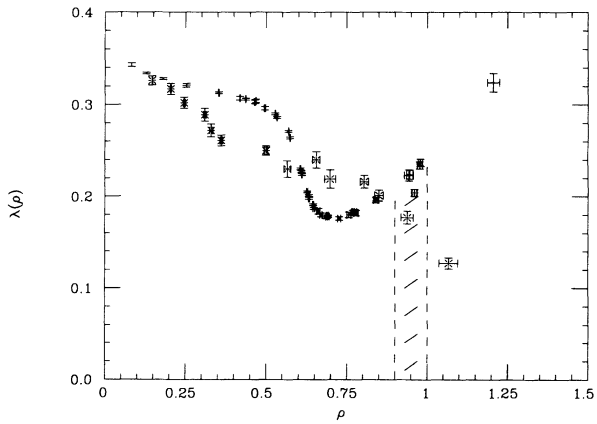

FIG. 5. The variational parameter λ as a function of ρ for twelve quarks. The eight quark results from Fig. 2 are shown as well, so that the the finite size effects may be seen more clearly. The twelve quark data are denoted by "×." The points indicate the optimum finite λ solutions as a function of density, and the associated errors bars are indicated. The hatched region indicates a transition region from finite to zero λ, and its width is 2σ, where sigma is the error assigned to the transition density estimate. This estimate is identical to that of the eight quark case.

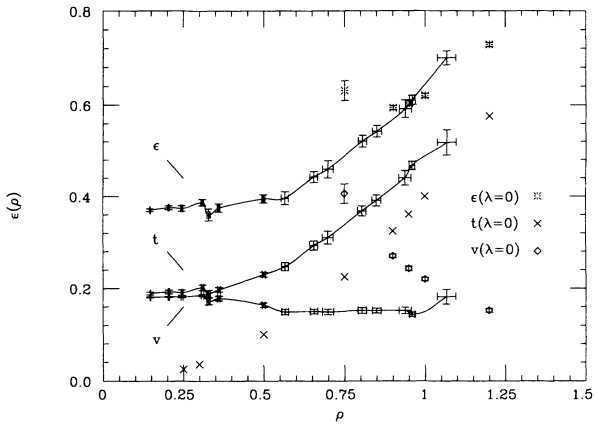

FIG. 6. The energy per particle $\varepsilon(\rho)$ as a function of ρ for twelve quarks. The notation is as per Fig. 4.

with the behavior of λ in this density regime. The twelve quark λ decreases smoothly to the transition region—the dip behavior seen in the eight quark case is absent.

We can now compare the results of the full SU(2) calculation, which we have just presented, to the results of the approximate SU(2)$_c$ treatment – the "painted model" described in Sec. IV. Figure 7 shows the optimum variational parameter in the painted model as a function of density for eight and twelve quarks. Here, as above, the variational parameter approaches the isolated hadron limit at low densities. At high densities, however, λ flows smoothly to zero; there is no abrupt transition to zero λ in this model. The finite size effects are small for $\rho \lesssim 0.6$; they only become significant at higher densities. If finite size effects are to exist in an isolated density regime, then it is sensible that they should exist only at larger densities. The variational parameters of the models do *not* bear closer comparison; the *Ansätze* from which they are derived are decidedly different.

The energy per particle in the painted model is shown as a function of density in Fig. 8 for eight and twelve

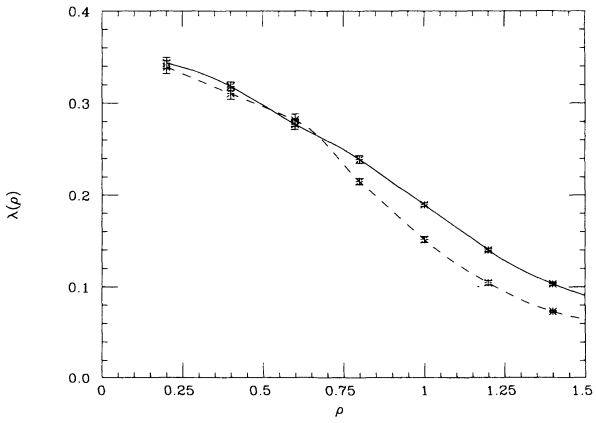

FIG. 7. The optimum variational parameter λ in the painted model, Eq. (4.3), as a function of density for eight and twelve quarks. The curves are merely to guide the eye. The dashed curve connects the eight quark calculations, whereas the solid curve connects the twelve quark ones.

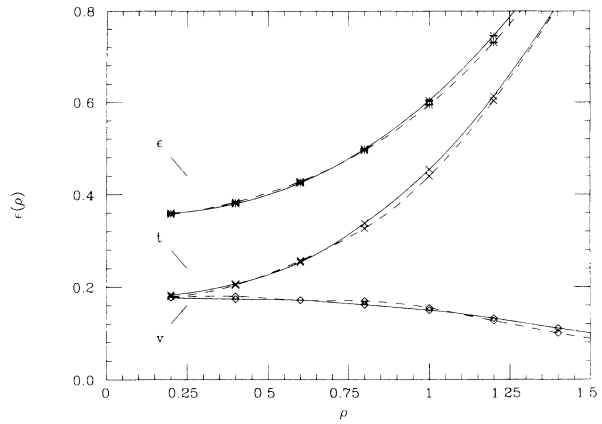

FIG. 8. The energy per particle as a function of density in the painted model for eight and twelve quarks. The curves are merely to guide the eye. As in Fig. 7, the dashed line connects the eight quark calculations, and the solid line connects the twelve quark ones. The statistical errors that are not shown are negligible relative to the scale of the figure. The remaining notation is as in Fig. 4.

quarks. The model results approach the isolated hadron limit at low density and the free Fermi gas limit at high density. As above, the potential energy tends slowly to zero as the density increases. Here the finite size effects are small—even at larger densities. The total energies per particle in the magic and painted models are compared in Fig. 9. The twelve quark calculations in the two models are fairly similar, even though the physics of the models is rather different. In comparing Figs. 6 and 8, we note that differences in t and v exist, but they tend to compensate. The similarity of the total energy per particle in the twelve quark cases does tend to support the use of the painted model for calculations of this ilk. It would be interesting to see if this similarity survives in calculations with more quarks.

B. Ground state structure

We shall now turn to a study of the system's ground state structure as a function of density. Figures 10 and 11 illustrate the two-body density versus the interquark separation r for various one-body densities in the eight and twelve quark cases. Both the calculations in the full and approximate $SU(2)_c$ models are shown; we hope that their comparison will yield further insight into the structure of the ground state. We shall consider the eight quark results, Fig. 10, first. Figure 10 shows the two-body density from low to high [(a)→(d)] density. Both the magic and painted models approach the isolated hadron limit at low density, as they should, although the painted model approaches the limit more quickly as ρ decreases. Note that in all cases $\rho_2(r)$ approaches one for sufficiently large r. The two-body density for the full $SU(2)_c$ case is shown at still lower density in Fig. 12(a); $\rho_2(r)$ does approach the isolated hadron limit at low density, as claimed. The painted model's more rapid approach to the isolated hadron limit can be readily understood through analyzing the models' *Ansätze*. Equations (4.8) and (4.9) show the structure of the two ground states as two quarks of the same color approach each other. The healing of the Fermi wound in the magic model contains an additional L-independent term; this is likely why the painted model approaches the isolated

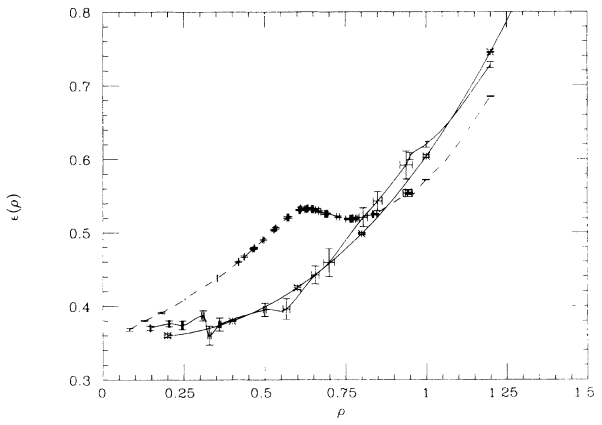

FIG. 9. The energy per particle in the magic [full SU(2)] and painted [approximate SU(2)] models as a function of density for eight and twelve quarks. The starred data points joined by the solid curve are the twelve quark painted model calculations from Fig. 8. The other solid curve connects the twelve quark magic model calculations from Fig. 6. The dashed curve joins the corresponding eight quark calculations from Fig. 4. Note that the energy per particle in the full SU(2) calculation is for the optimal variational parameter solution; λ is not required to be finite.

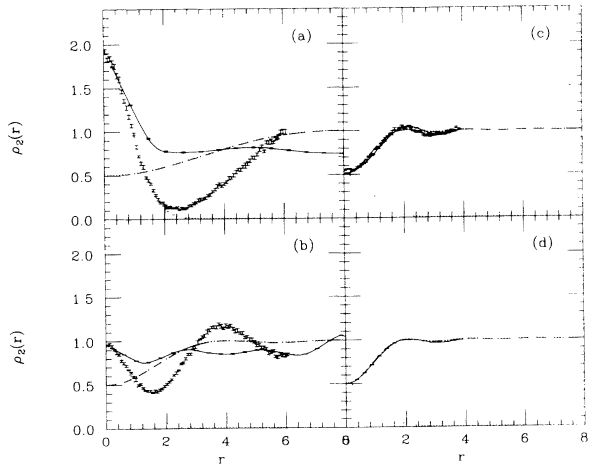

FIG. 10. The two-body density as a function of the interquark separation r for a variety of densities for the eight quark case. Both the results of the full (magic) and approximate SU(2) (painted) calculations have been plotted. The full SU(2) points are joined by a solid line to guide the eye. The dashed curve is the two-body density appropriate to a free Fermi gas [Eq. (5.26)], and the dotted curve shows that appropriate to the isolated hadron limit [Eq. (5.23)]. Note that in (a) $\rho = 0.25$, in (b) $\rho = 0.50$, in (c) $\rho = 0.95$, and λ is the optimum finite solution, and in (d) $\rho = 0.95$ and $\lambda = 0$.

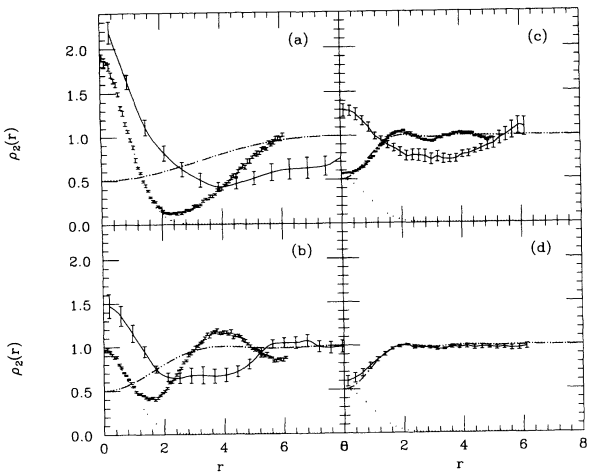

FIG. 11. The two-body density as a function of the interquark separation r for a variety of densities for the twelve quark case. The notation is identical to that of Fig. 10.

hadron limit more quickly. At moderate density, $\rho = 0.5$, the full and approximate SU(2) calculations are quite different, although there is no reason why they should be the same. At still higher densities, the two models are again similar, but that is because they are approaching the Fermi gas limit. At $\rho = 0.95$, λ in the painted model is small, but finite, and the corresponding two-body density is nearly that of a free Fermi gas. The same is true of the magic model, although λ exhibits a rapid drop to zero in this density regime. The finite λ two-body density in (c) is only slightly different from the zero λ result in (d); apparently the structure of the state changes little across the "transition." The result in (d) is essentially identical to the free Fermi gas result; this implies that the finite-size effects are under some measure of control. We can explore this issue directly by studying the twelve quark results in Fig. 11.

The finite-size effects in $\rho_2(r)$ under the change from eight to twelve quarks are significant in the magic model, although they are modest in the painted model. Note that the zero λ two-body density in (d) shows reasonable agreement with the free Fermi gas result: the finite-size effects are in the finite λ calculation. Perhaps the *Ansatz* of Eq. (3.15) is ineffective in describing the additional correlation the quarks feel due to confinement

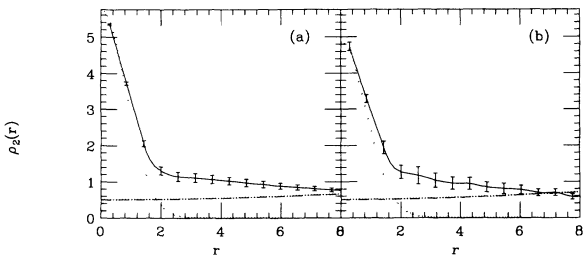

FIG. 12. The two-body density as a function of the interquark separation r for the full SU(2)$_c$ calculation—the "magic" model—in the low density limit. Case (a) is for eight quarks with $\rho = 0.08$, and case (b) is for twelve quarks with $\rho = 0.1$. In each case, the dotted line corresponds to the appropriate isolated hadron two-body density.

at moderate density. In particular, the two-body density now changes as λ changes from its optimum finite value to zero at the transition density. In general, $\rho_2(r)$ in the magic model has additional strength at $r = 0$, compared to the eight quark results. This calculation still appears to satisfy the isolated hadron limit, however, as shown in Fig. 12(b). The ground state structure of the painted and magic models at the twelve quark level appears to be rather different. As in the eight quark case, the painted model approaches the isolated hadron limit much more rapidly. The differing structure of the two models' *Ansätze*, Eqs. (4.8) and (4.9), as two quarks of the same color approach each other, is likely responsible for this effect. The nature of the correlations included in the painted and magic model are different, and the two-body density is apparently quite sensitive to those differences. It would be interesting to see whether this sensitivity would be preserved in calculations performed with still more quarks.

The approach of the magic model to the isolated hadron limit, as shown in Fig. 12, serves to illustrate another point concerning the structure of the state. At small r, the Monte Carlo calculations of the two-body density track the isolated hadron results fairly closely. At larger r, however, there is a significant "filling-in" of the two-body density relative to the isolated hadron result. This is in contrast to the painted model calculations at low density, as depicted in Figs. 10(a) and 11(a). There the two-body density tracks the isolated hadron result until it reaches essentially zero; it eventually picks up again because other hadron clusters exist at finite density. The difference in the behavior of the two models as r increases in the low density limit arises from the exchange terms included in the magic model. For any fixed, finite density, there exists some r for which the exchange term to recouple a quark pair into different hadrons is finite. Such terms do not exist in the painted model as the colors of the quarks are fixed. This effect explains the "wings" seens on the two-body density in the magic model shown in Fig. 12.

We can understand the difference between the magic and painted models at low densities in yet another way. That is, the large dip below one in the painted model's $\rho_2(r)$ at large r can be interpreted in terms of a repulsive effective force between hadron clusters in this model. This is simply due to antisymmetry. A red quark in one cluster must be anticorrelated with the red quark it sees in an adjacent cluster. In the magic model, the inclusion of exchange terms allows some additional attraction to exist, since the colors of the quarks can change. As a red quark in one cluster approaches a red quark in an adjacent cluster, the first quark can flip its color and pair off with the red quark it approaches. In this way the effective attraction—relative to the painted model—is generated.

We have now completed our survey of results in the full SU(2)$_c$ model.

VII. SUMMARY AND OUTLOOK

Here we have considered nuclear matter in the context of a nonrelativistic constituent quark model with an internal color degree of freedom. In part, we have been

motivated by a desire to understand traditional issues, such as nuclear matter binding and saturation, from a quark model viewpoint. Our primary interest, however, is in the properties of the system as a function of density. The model system we consider becomes a gas of isolated hadrons at low density, and a nonrelativistic free Fermi gas at high density. Thus, it provides a natural laboratory in which to understand how the combined effects of confinement and antisymmetry determine the structure of the system as it evolves between the two limits. In particular, we wish to gain insight into a possible "deconfinement" phase transition at high density.

The model we consider is a simple one. It is derived from the combined application of the adiabatic and strong coupling limits to QCD, and it consists of the following prescription: the quarks are always paired to the lowest energy set of flux tubes. Consequently, the model contains no dynamical gluon degrees of freedom; the dynamics are those of quark exchange. We remind the reader that the global minimization prescription which defines our model also guarantees that it is free from residual color van der Waals forces—an advantage over two-body potential models in three dimensions [14]. The model is nonrelativistic, although we are, in principle, interested in density regimes in which relativistic effects could be important. We feel that the model's simplicity and intrinsic appeal outweighs its disadvantages for the qualitative purposes of our study. Its primary advantage is that it places quark and hadron degrees of freedom on an equal footing. The structure of the system at intermediate densities is due entirely to the model dynamics, namely of confinement and antisymmetry, rather than to the heuristic approximations obliged in a more complicated model.

The quark exchange model has been used in previous studies of nuclear matter [5–10]. Our contribution here has been the complete incorporation of an internal SU(2) color degree of freedom, although we have continued to ignore the quarks' spin. By "complete," we mean that we have incorporated the internal degree of freedom without giving the quarks *fixed* colors. This is important: QCD requires that a many-quark system be an overall color singlet, but it does not determine the colors of the individual quarks. We have constructed an explicitly antisymmetric variational *Ansatz* with the internal degree of freedom, and then proceeded with a Monte Carlo calculation to determine the properties of the system.

We have found that the $SU(2)_c$ results look rather different from earlier "spin 0 fermion" studies [5,6]. Indeed, the simulations support an abrupt transition from finite to zero variational parameter, which describes the system's clustering into hadrons, at moderately high density. The system with zero variational parameter is a free Fermi gas. The change of the structure of the system across this transition is sensitive to finite-size effects. At the eight quark level, the two-body density changes little as the variational parameter changes from its optimum finite value to zero at the transition density. However, the same calculation performed at the twelve quark level shows a significant effect. A definitive conclusion as to the structure of the system as it goes through the transition regime must be reserved, then, for later study. This abrupt change in the variational pararmeter as a function of density is also absent in the "painted"—the quarks have fixed colors—SU(2) study we considered here for comparison. It would be interesting to see if this effect persists in three spatial dimensions and in full SU(3) color.

The energy per particle as a function of density in this model shows rich behavior as a function of density. At moderate densities, the system is capable of tolerating longer string lengths in order to reduce its kinetic energy. We should note, in passing, that in a model with linear, rather than harmonic, confinement these effects would likely be more pronounced. The energy per particle rises more slowly with density than those of earlier studies without color, but nuclear matter in this model is not bound. The energy per particle does become considerably flatter with density under the change from eight to twelve quarks, however. The change is, in fact, big enough that the existence of a bound state cannot be ruled out as the number of quarks increases. Yet, the lack of a bound state in our twelve quark calculation is hardly a surprise. The dynamics in this model are simple and do not suffice to reproduce the known features—such as the spin dependence—of the N-N force.

Unlike the full SU(2) model, the painted SU(2) calculation of the energy per particle shows small finite size effects under the change from eight to twelve quarks. The twelve quark energy per particle results in the full and painted SU(2) calculations are surprisingly similar. This is in contrast to the evolution of the variational parameter and two-body density of the two calculations with density, which are different. It would be interesting to see whether this similarity persists in a calculation with more quarks. The similarity which does exist, however, lends support to the further use of the painted model in exploring the energetics of bulk quark matter, for example, when flavor degrees of freedom are included [26]. However, the distinctly different two-body densities in the two models indicate that a complete treatment of antisymmetry is necessary to understanding the system's ground state structure. Indeed, this may also indicate that a complete incorporation of spin and flavor degrees of freedom as well are essential to an understanding of the ground state of hadronic matter with density.

The computation of the two-body density in this model has given us insight into the structure of the ground state as a function of density. In principle, we would also like to study the excitations of the system as well. We can explore the "phonon-like" behavior of the system through the calculation of the Fourier transform of the two-body density [27]. It is possible, however, to gain access to the full response of the system. That is, we can calculate the quark response function in imaginary time, and then reconstruct the longitudinal response function, familiar from inclusive electron scattering, by finding the inverse Laplace transform of the Euclidean response. The inversion procedure is nonunique, but Carlson and Schiavilla [28] have shown it practicable for light nuclei. We imagine that the quark response function would evince rich behavior as a function of density.

ACKNOWLEDGMENTS

We thank B. Serot for a critical reading of the manuscript. This research was supported by the AAUW Educational Foundation (S.G.), by the DOE under Contracts No. DE-AC05-84ER40150 (S.G.) and No. DE-FG02-87ER40365 (S.G. and C.J.H.), and by the Florida State University Supercomputer Computations Research Institute through the DOE Contracts Nos. DE-FC05-85ER250000 and DE-FG05-92ER40750 (J.P.).

[1] T. Matsui and H. Satz, Phys. Lett. B **178**, 416 (1986).
[2] S. Gavin, M. Gyulassy, and A. Jackson, Phys. Lett. B **207**, 257 (1988).
[3] J. Hüfner, Y. Kurihara, and H. J. Pirner, Phys. Lett. B **215**, 218 (1988).
[4] F. Lenz, J. T. Londergan, E. J. Moniz, R. Rosenfelder, M. Stingl, and K. Yazaki, Ann. Phys. (N.Y.) **170**, 65 (1986).
[5] C. J. Horowitz, E. J. Moniz, and J. W. Negele, Phys. Rev. D **31**, 1689 (1985).
[6] C. J. Horowitz and J. Piekarewicz, Phys. Rev. C **44**, 2753 (1991).
[7] C. J. Horowitz and J. Piekarewicz, Nucl. Phys. **A536**, 669 (1992).
[8] P. J. S. Watson, Nucl. Phys. **A494**, 543 (1989); A. B. Migdal and P. J. S. Watson, Phys. Lett. B **252**, 32 (1990).
[9] W. M. Alberico, M. B. Barbaro, A. Molinari, and F. Palumbo, Z. Phys. A **341**, 327 (1992); W. M. Alberico, M. B. Barbaro, A. Magni, and M. Nardi, Nucl. Phys. **A552**, 495 (1993).
[10] G. M. Frichter and J. Piekarewicz, Comput. Phys. **8**, 223 (1994).
[11] S. Gardner and E. J. Moniz, Phys. Rev. C **36**, 2504 (1987); S. Gardner, *ibid.* **42**, 2193 (1990).
[12] M. Lissia and J. W. Negele, Phys. Rev. D **39**, 1413 (1989).
[13] G. Feinberg and J. Sucher, Phys. Rev. D **20**, 1717 (1979).
[14] O. W. Greenberg and H. J. Lipkin, Nucl. Phys. **A370**, 349 (1981).
[15] N. Isgur and J. Paton, Phys. Rev. Lett. **54**, 869 (1985).
[16] N. Isgur, in *The New Aspects of Subnuclear Physics*, edited by A. Zichichi (Plenum, New York, 1980).
[17] M. Harvey, J. Letourneux, and B. Lorazo, Nucl. Phys. **A424**, 428 (1984).
[18] K. Maltman and N. Isgur, Phys. Rev. D **29**, 952 (1984).
[19] J. H. Weis, Acta Phys. Pol. B **9**, 1051 (1977); J. Ellis, *ibid.* **8**, 1019 (1977).
[20] S. Huang, J. W. Negele, and J. Polonyi, Nucl. Phys. **B307**, 669 (1988), and references therein.
[21] M. Engelhardt and B. Schreiber, "Elimination of Color in 1 + 1-dimensional QCD," University of Erlangen-Nürnberg report, 1994.
[22] F. Lenz, M. Thies, S. Levit, and K. Yazaki, Ann. Phys. (N.Y.) **208**, 1 (1991).
[23] I. Bars and M. B. Green, Phys. Rev. D **17**, 537 (1978).
[24] R. E. Burkard and U. Derigs, *Lecture Notes in Economics and Mathematical Systems* (Springer-Verlag, Berlin, 1980), vol. 184.
[25] N. Isgur and G. Karl, Phys. Rev. D **20**, 1191 (1979).
[26] J. Piekarewicz, in preparation.
[27] R. P. Feynman, *Statistical Mechanics* (Addison-Wesley, Reading, 1972), p.328ff.
[28] J. Carlson and R. Schiavilla, Phys. Rev. Lett. **68**, 3682 (1992).

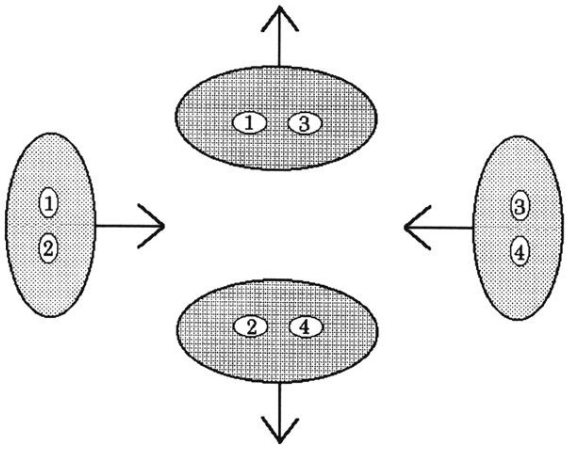

FIG. 1. An illustration of quark exchange dynamics for four quarks. Two incoming hadrons with quark content $(12)_0$ and $(34)_0$ may exchange quarks—the strings connecting 1 to 2 and 3 to 4 flip—to yield a $(13)_0(24)_0$ outgoing state.